Applied Physics Letters ARTICLE pubs.aip.org/aip/apl

Acoustic chiral mode switching by dynamic encircling of exceptional points

Cite as: Appl. Phys. Lett. **123**, 101701 (2023); doi: 10.1063/5.0163290
Submitted: 16 June 2023 · Accepted: 17 August 2023 ·
Published Online: 5 September 2023

Youdong Duan,[1] Linlin Geng,[1,a)] Qiuquan Guo,[2] Jun Yang,[2] Gengkai Hu,[1] and Xiaoming Zhou[1,a)]

AFFILIATIONS

[1]Key Laboratory of Dynamics and Control of Flight Vehicle of Ministry of Education, School of Aerospace Engineering, Beijing Institute of Technology, Beijing 100081, China
[2]Shenzhen Institute for Advanced Study, University of Electronic Science and Technology of China, Shenzhen 518110, China

[a)]**Authors to whom correspondence should be addressed:** genglinlin@bit.edu.cn and zhxming@bit.edu.cn

ABSTRACT

Chiral mode switching initiated by dynamic encircling of an exceptional point (EP) has shown an extraordinary ability in wave controlling. In this work, we study the chiral mode transfer for acoustic waves in the coupled waveguide system that supports the non-adiabatic evolution of eigenstates. The system comprises a finite number of structural elements, which are constructed according to parametric conditions in the loop enclosing the EP and then stacked such that acoustic propagation in the waveguide system is equivalent to the dynamic encircling of the EP. An analytic model based on the spatial coupled-mode theory is developed, which provides a practical guide to design the system and makes predictions for dynamic evolution. Numerical simulation of the waveguide system is conducted to demonstrate the chiral mode switching for sounds.

Non-Hermitian systems have attracted considerable attention in recent years.[1,2] They were shown to possess many fascinating properties such as exceptional point (EP),[3] enhanced sensing,[4,5] and non-Hermitian skin effect.[6] The EP refers to a branch singularity at which both eigenvalues and eigenvectors coalesce simultaneously and is one of the core concepts in non-Hermitian physics. The Riemann topological structure of the eigenvalue surface is a behavior of particular interest associated with the EP. It activates the study of eigenmode evolution in paths encircling the EP and has led to many novel phenomena.[7,8] Adiabatically encircling the EP along a loop in parameter space results in the flipping of eigenstates. More interestingly, non-adiabatically encircling an EP exhibits an intriguing chiral mode switching phenomenon,[9] which is immune to the path irregularity as long as the EP is enclosed.

Recently, there grows a great interest in extension of non-Hermitian physics to acoustic systems in order to develop unusual acoustic-control applications.[10] Acoustic EPs can be generated in cavity or waveguide structures with the loss and/or gain elements. Thanks to the design flexibility of an acoustic platform, more complex EP phenomena, including anisotropic EP,[11] higher-order EP,[12] and exceptional nexus,[13] have been unveiled and accompanied by richer eigenvalue topological structures. Topological properties can be inferred from the mode profiles during the adiabatic evolution of eigenstates around EPs. To achieve this goal, these systems are constructed and measured separately at various parametric points in order to prevent non-adiabatic transition. Inherently, these models are not compatible with the dynamic encircling of EPs. Acoustic chiral mode transfer relying on non-adiabatic evolution has not yet been well demonstrated.

The dynamic evolution of eigenstates can be achieved by a Hamiltonian that evolves continuously with time as usually worked with non-Hermitian quantum systems.[14] By analogy with this phenomenon, the chiral transfer of vibration modes has been proposed in a two-state mechanical system by the time-driven non-adiabatic encircling of EPs.[15] However, extension of this strategy to acoustics is still challenging as it relies on the time-modulation of sounds. As an alternative approach, the space-propagation evolution of the eigenstate, which is equivalent to the time-evolution scenarios,[16,17] has been used to realize the chiral mode switching in microwave[18] and photonic waveguide systems.[19] Acoustic counterpart of chiral mode switching by space evolution remains under-explored, which is expected to generate unusual wave manipulation strategies in acoustic communication and signal processing. In this work, we report the design of spatially coupled acoustic systems and prove acoustic chiral mode switching induced by the spatially driven dynamic encircling of an EP.

Consider a coupled waveguide system as shown in Fig. 1, which is composed of two individual waveguides coupled through narrow tubes arranged periodically. The basic element of the system consists of two cavities with height h, width a, and length L, connected by a tube of width w and length L_c. Acoustic impedance conditions Z_1 and Z_2 are set for two cavities at a circular area of radius R. The energy gain or drain can be acquired by setting negative or positive acoustic resistances in the impedance boundary in order to introduce the non-Hermitian effect. Such kind of the impedance condition is potentially realizable through loudspeakers with shunting circuits[20–22] (see the supplementary material for details).

The wave propagation in the coupled waveguide system can be described by the spatial coupled-mode equation,[23]

$$i\frac{d}{dz}\Psi(z) = \mathbf{H}\Psi(z), \quad \mathbf{H} = \begin{bmatrix} \beta_1 + i\gamma_1 & \kappa \\ \kappa & \beta_2 - i\gamma_2 \end{bmatrix}, \tag{1}$$

where $\Psi(z) = [A_1(z), A_2(z)]^{\mathrm{T}}$ with A_1 and A_2 denoting pressure fields in a two sub-waveguide system. $\mathbf{H}$ represents the Hamiltonian of the system, where the diagonal terms $\beta_1 + i\gamma_1$ and $\beta_2 - i\gamma_2$ denote the complex wavenumber of two individual waveguides, and the off diagonal term κ describes the coupling magnitude of two propagation modes. The correlation between the Hamiltonian parameters and structural parameters of the waveguide system can be established based on the fitting method as given in the supplementary material. Given an excitation frequency, the complex wavenumber of the individual waveguide can be managed by the surface impedance, while the coupling magnitude κ depends on the connection tube. This simple mapping relationship facilitates the design of acoustic systems with dynamic encircling of an EP.

The EP condition of the acoustic system can be derived by solving the eigenvalue problem of Eq. (1). The eigenvalue λ and corresponding eigenvector ψ are calculated as

$$\lambda_{1,2} = \frac{\beta_+ + i\gamma_- \mp \sigma}{2}, \quad \psi_{1,2} = \left[\frac{-\beta_- + i\gamma_+ \mp \sigma}{2\kappa}, 1\right]^{\mathrm{T}}, \tag{2}$$

where $\beta_{+,-} = \beta_2 \pm \beta_1, \gamma_{+,-} = \gamma_1 \pm \gamma_2$, and $\sigma = \sqrt{4\kappa^2 - (\gamma_+ + i\beta_-)^2}$. According to Eq. (2), the condition for EP to occur is $\sigma = 0$, which results in $\beta_- = 0$ and $\gamma_+ = 2\kappa$. By use of this condition, the waveguide system possessing an EP can be designed with help of the fitting method. The structural parameters of the designed EP system are $a = 6$ cm, $L = 15$ cm, $h = 8$ cm, $w = 2.56$ mm, $L_c = 3$ cm, and $R = 1.95$ cm. Acoustic impedance is set as $Z_1 = \rho_0 c_0(-5 + i)$ and $Z_2 = \rho_0 c_0(5 + i)$, where the air density $\rho_0 = 1.21\,\mathrm{kg/m^3}$ and sound velocity $c_0 = 343$ m/s are used. The excitation frequency is chosen as $f = 1800$ Hz. The fitting results of Hamiltonian parameters are $\beta_1 = \beta_2 = 32.9$ rad/m and $\gamma_1 = \gamma_2 = \kappa = 0.16$ rad/m, which satisfy the EP condition.

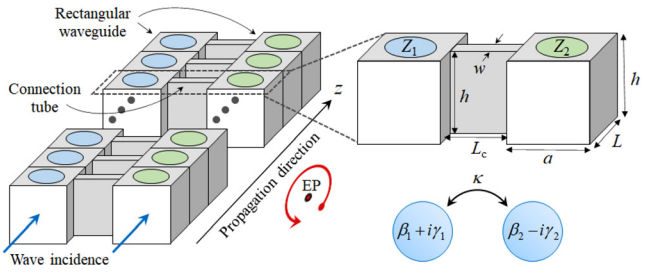

FIG. 1. Schematic diagram of the acoustic waveguide system that supports the dynamic evolution of eigenstates around an exceptional point.

We proceed to examine the variation in eigenvalues near the EP in parameter space of coordinates β_1 and κ as shown in Figs. 2(a) and 2(b). Note that $\beta_2 = 32.9$ rad/m and $\gamma_1 = \gamma_2 = 0.16$ rad/m are kept unchanged upon the variation of β_1 and κ. It is seen from Fig. 2(a) that the imaginary part pattern comprises two sheets that are symmetric about the zero plane. The mode with $\mathrm{Im}(\lambda) < 0$ is purely lossy, while the other mode with $\mathrm{Im}(\lambda) > 0$ is of gain. They represent, respectively, the propagating waves with the decaying and growing amplitudes and are termed here as L and G modes for brevity. These two modes coalesce at the parity-time (PT) symmetric phase line, where their corresponding real parts bifurcate, forming the branch cut. At this line, the eigenmode remains unchanged, $\mathscr{P}\mathscr{T}\boldsymbol{\psi}_{1,2} = \boldsymbol{\psi}_{1,2}$, after the action of the parity-time operator ($\mathscr{P}\mathscr{T}$). Figure 2(c) shows the typical modal field of the symmetric phase mode. The energy is evenly distributed in two cavities. The field distribution is symmetric for the G mode while it is anti-symmetric for the L one.

The real parts of eigenvalues are characterized by self-intersecting Riemann surfaces, as shown in Fig. 2(b). They coalesce at the line of the PT-broken phase, where one mode can be transformed into another by $\mathscr{P}\mathscr{T}$ operation through $\mathscr{P}\mathscr{T}\boldsymbol{\psi}_{1,2} = \boldsymbol{\psi}_{2,1}$. As a signature of these eigenmodes, the energy is unevenly distributed in two cavities as shown in Fig. 2(d). The eigenvalue Riemann surface shown in Fig. 2 has exhibited the same topology as that in PT-symmetric systems.[18] Therefore, we may expect the chiral mode switching for symmetric phase modes in the process of dynamic encircling of the EP.

In the wave propagation model, space coordinate z plays the same role of time in the time evolution case,[17] such that the dynamic encircling of the EP can be implemented by the space(z)-driven evolution of $\beta_1(z)$ and $\kappa(z)$. The evolution path is chosen as the closed loop parameterized by

$$\beta_1(z) = -0.2\sin\phi(z) + \beta_0, \quad \kappa(z) = 0.2\cos\phi(z) + \kappa_0, \tag{3}$$

where $\beta_0 = 32.97$ rad/m, $\kappa_0 = 0.25$ rad/m, and $\phi(z) = 2\pi z/L_t$ with L_t denoting the total evolution length in the z direction. In Eq. (3), the start point with the symmetric-phase feature has been warranted as

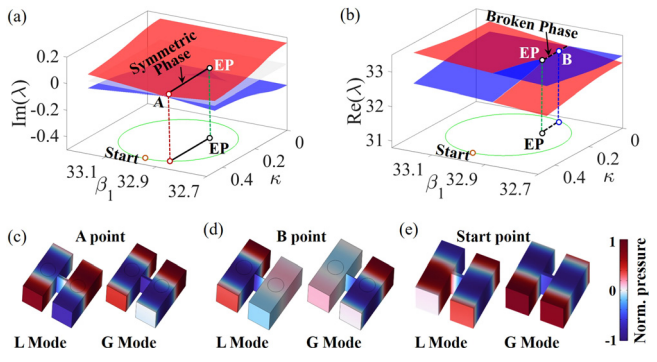

FIG. 2. (a) Imaginary and (b) real parts of eigenvalues in parameter space (β_1, κ); field pattern of eigenmodes at (c) the symmetric-phase point, (d) broken-phase point, and (e) start point of dynamic evolution.

shown in Fig. 2(e). The realistic system with the dynamic evolution comprises a finite number of elements. Here, the parametric loop is discretized into $N = 140$ points with coordinates $z_j = jL$ $(j = 0, \ldots, N-1)$. At various parametric points $\beta_1(z_j)$ and $\kappa(z_j)$, the elementary structure is constructed by modulating Z_1 and w, while keeping other structural parameters unchanged. Then, all elements are stacked along the z direction so that acoustic propagation in the waveguide system is equivalent to the dynamic evolution enclosing the EP. The anti-clockwise (clockwise) evolution along the loop corresponds to the wave propagation toward the positive (negative) z direction.

Acoustic propagation simulations are performed based on COMSOL Multiphysics to evaluate the eigenmode evolution under different conditions of input states and loop directions. Take the L mode injection and anti-clockwise evolution as an example, this input condition can be implemented by applying the radiation boundary condition to the z_0-element of the system, where the source pressure is taken from the L mode at the starting point of the loop. The output port at the far side of the system is terminated by nonreflecting boundaries. Modal amplitudes of L and G modes in the dynamic evolution process can be retrieved from simulation results by the following procedure. Denote the domain occupied by the jth element as Ω_j, and two cavities in this element are further represented by $\Omega_{j,1}$ and $\Omega_{j,2}$. The corresponding pressure fields obtained from numerical simulation are denoted by $P_{j,1}(\Omega_{j,1})$ and $P_{j,2}(\Omega_{j,2})$. Now express $\Phi_j = [P_{j,1}, P_{j,2}]^{\mathrm{T}}$ in terms of eigenmode bases $\psi_{\mathrm{L},j}(\Omega_j)$ and $\psi_{\mathrm{G},j}(\Omega_j)$ as[16]

$$\Phi_j = q_{\mathrm{L},j}\psi_{\mathrm{L},j} + q_{\mathrm{G},j}\psi_{\mathrm{G},j}, \tag{4}$$

where $q_{\mathrm{L},j}$ and $q_{\mathrm{G},j}$ are modal amplitudes of the interest. Details to calculate the modal amplitude are given in supplementary material.

Figure 3 shows the variation in modal amplitudes along z in four cases with different input states and evolution directions. In all cases, the modal amplitude curve is subject to an abrupt change corresponding to the branch cut (BC). Apart from this signature, the curve crossing phenomenon, also known as a non-adiabatic transition (NAT),[24] occurs in selective cases of Figs. 3(b) and 3(c). This behavior is inherently related to the non-adiabatic coupling among eigenmodes. Here, an intuitive understanding to the NAT behavior is provided from the perspective of wavenumber eigenvalues. Remind that the L or G wave modes have the decaying or amplifying nature. In Figs. 3(b) and 3(c), the L mode is dominant before the NAT to occur. With the decaying nature, its amplitude gradually decreases and tends to intersect the G mode curve with the growing amplitude, eventually forming the NAT at a specific point. The absence of the NAT in Figs. 3(a) and 3(d) may be understood by the fact that the G mode is dominant at the early stage of dynamic evolution, and it continues to dominate the evolution due to its amplifying nature such that two curves always keep separate.

The dynamic evolution in the waveguide system can also be predicted in theory according to Eq. (1) by replacing the Hamiltonian with the z-dependent one,

$$\mathbf{H}(z) = \begin{bmatrix} \beta_1(z) + i\gamma_1 & \kappa(z) \\ \kappa(z) & \beta_2 - i\gamma_2 \end{bmatrix}. \tag{5}$$

Theoretical predictions of modal amplitudes have been plotted in Fig. 3 and are in good agreement with simulation results. Slight deviations from simulation results can be attributed to the coupled-mode approximation and fitting error of the Hamiltonian parameters. It is

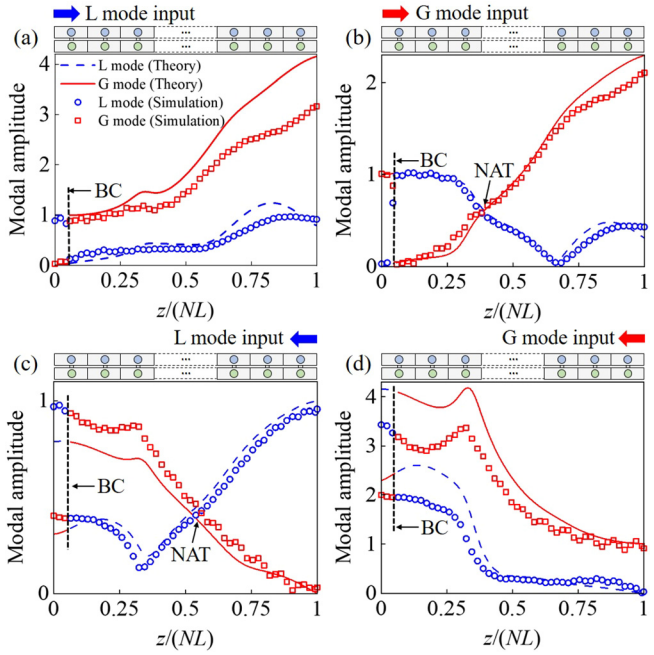

FIG. 3. Simulation and theoretical results of modal amplitudes of L and G modes in the process of dynamically encircling the EP in four cases: (a) the L mode input and anti-clockwise evolution; (b) the G mode input and anti-clockwise evolution; (c) the L mode input and clockwise evolution; (d) the G mode input and clockwise evolution.

concluded from Fig. 3 that the system outputs the G mode for the anti-clockwise evolution case, while exports the L mode for the clockwise evolution case. This mode transferring behavior, which is decided by the evolution direction, while irrelevant to the input state, is referred to as the chiral mode switching,[9] and is consistent with the phenomenon in the time-driven evolution scenario.[15]

Chiral mode transfer can be further confirmed by examining pressure phase information of input and output elements. Denote the phase difference between two cavities by $\Delta\theta$. Figure 4 plots the variation of $|\Delta\theta|/\pi$ in the waveguide system. The start/end point locates near the symmetric-phase line. So, two cavities in input and output elements should be either out of phase $|\Delta\theta|/\pi \approx 1$ (L mode) or in phase $|\Delta\theta|/\pi \approx 0$ (G mode), depending on the result of chiral switching. It can be observed from Fig. 4 that the clockwise evolution around the EP ends with the L mode, while the G mode is obtained at the end of the anti-clockwise evolution. Theoretical predictions coincide very well with simulation results, clearly demonstrating acoustic chiral mode switching.

In summary, acoustic non-adiabatic encircling of an EP is studied in a coupled waveguide system. An analytic model is established based on the spatial coupled-mode theory to describe the dynamic evolution of eigenstates. We first construct a PT-symmetric EP and then design a waveguide system according to a parametric loop enclosing the EP such that acoustic propagation in the system is equivalent to the dynamic encircling of the EP. Both theoretical and numerical results demonstrate acoustic chiral mode switching. Apart from proving acoustic chiral dynamics, this work provides a platform for exploring

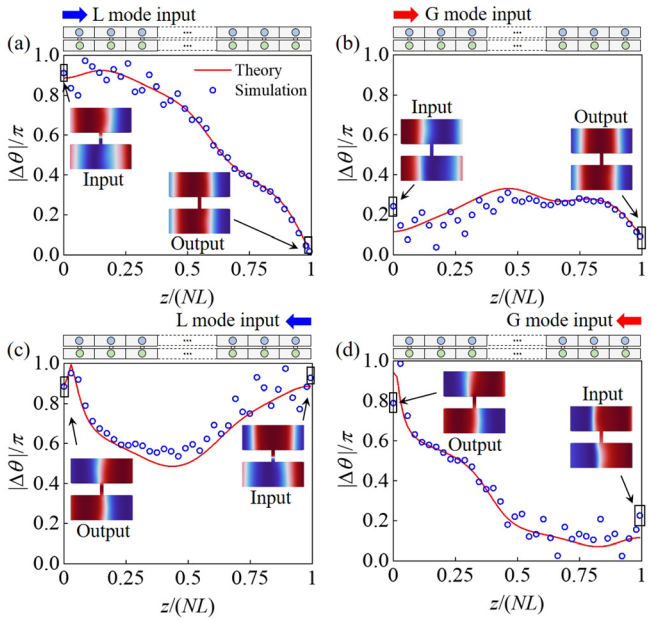

FIG. 4. (a)–(d) Simulation and theoretical results of $|\Delta\theta|/\pi$ in the waveguide system, corresponding to four cases in Figs. 3(a)–3(d), respectively. The insets show the pressure field distribution for input and output elements.

the non-adiabatic coupling behavior of sounds, which may contribute to the observation of other quantum-like behaviors.

See the supplementary material for more details on the potential realization of acoustic impedance conditions Z_1 and Z_2, the fitting method of Hamiltonian parameters, and the calculation method of modal amplitudes.

This work was supported by the National Natural Science Foundation of China (Nos. 12225203, 11622215, 11872111, 11991030, and 11991033), the 111 Project (B16003), and the Shenzhen Science and Technology Program (Nos. JCYJ20210324115412035 and ZDSYS20210813095534001).

AUTHOR DECLARATIONS

Conflict of Interest

The authors have no conflicts to disclose.

Author Contributions

Youdong Duan: Investigation (equal); Methodology (equal); Validation (equal); Writing – original draft (equal). **Linlin Geng:** Conceptualization (equal); Investigation (equal); Methodology (equal); Validation (equal); Writing – original draft (equal). **Qiuquan Guo:** Investigation (equal); Writing – review & editing (equal). **Jun Yang:** Investigation (equal); Writing – review & editing (equal). **Gengkai Hu:** Investigation (equal); Writing – review & editing (equal). **Xiaoming Zhou:** Conceptualization (equal); Investigation (equal); Methodology (equal); Supervision (lead); Writing – original draft (equal); Writing – review & editing (equal).

DATA AVAILABILITY

The data that support the findings of this study are available from the corresponding authors upon reasonable request.

REFERENCES

[1]R. E. Ganainy, M. Makris, K. G. Khajavikhan, Z. H. Musslimani, S. Rotter, and D. N. Christodoulides, Nat. Phys. **14**(1), 11–19 (2018).
[2]Y. Yu, W. Song, C. Chen, T. Chen, H. Ye, X. Shen, Q. Cheng, and T. Li, Appl. Phys. Lett. **116**(21), 211104 (2020).
[3]M. A. Miri and A. Alu, Science **363**(6422), 7709 (2019).
[4]M. D. Carlo, F. D. Leonardis, R. A. Soref, L. Colatorti, and V. M. N. Passaro, Sensors **22**(11), 3977 (2022).
[5]J. Yuan, L. Geng, J. Huang, Q. Guo, J. Yang, G. Hu, and X. Zhou, Phys. Rev. Appl. **18**(6), 064055 (2022).
[6]X. Zhang, T. Zhang, M.-H. Lu, and Y.-F. Chen, Adv. Phys. X **7**(1), 2109431 (2022).
[7]C. Dembowski, B. Dietz, H. Graf, H. Harney, A. Heine, W. Heiss, and A. Richter, Phys. Rev. E **69**(5), 056216 (2004).
[8]C. Dembowski, H. Graf, H. Harney, A. Heine, W. Heiss, H. Rehfeld, and A. Richter, Phys. Rev. Lett. **86**(5), 787–790 (2001).
[9]R. Uzdin, A. Mailybaev, and N. Moiseyev, J. Phys. A: Math. Theor. **44**(43), 435302 (2011).
[10]Z. Gu, H. Gao, P. C. Cao, T. Liu, X. F. Zhu, and J. Zhu, Phys. Rev. Appl. **16**(5), 057001 (2021).
[11]K. Ding, G. Ma, Z. Q. Zhang, and C. T. Chan, Phys. Rev. Lett. **121**(8), 085702 (2018).
[12]K. Ding, G. Ma, M. Xiao, Z. Q. Zhang, and C. T. Chan, Phys. Rev. X **6**(2), 021007 (2016).
[13]W. Tang, X. Jiang, K. Ding, Y. X. Xiao, Z. Q. Zhang, C. T. Chan, and G. Ma, Science **370**(6520), 1077–1080 (2020).
[14]W. Liu, Y. Wu, C. K. Duan, X. Rong, and J. Du, Phys. Rev. Lett. **126**(17), 170506 (2021).
[15]L. Geng, W. Zhang, X. Zhang, and X. Zhou, Proc. R. Soc. A: Math. Phys. Eng. Sci. **477**(2245), 20200766 (2021).
[16]X. L. Zhang, S. Wang, B. Hou, and C. T. Chan, Phys. Rev. X **8**(2), 021066 (2018).
[17]R. Uzdin and N. Moiseyev, Phys. Rev. A **85**(3), 031804 (2012).
[18]J. Doppler, A. A. Mailybaev, J. Bohm, U. Kuhl, A. Girschik, F. Libisch, T. J. Milburn, P. Rabl, N. Moiseyev, and S. Rotter, Nature **537**(7618), 76–79 (2016).
[19]H. Xu, D. Mason, L. Jiang, and J. G. E. Harris, Nature **537**(7618), 80–83 (2016).
[20]R. Fleury, D. Sounas, and A. Alù, Nat. Commun. **6**, 5905 (2015).
[21]L. He, Y. Li, B. Djafari-Rouhani, and Y. Jin, Phys. Rev. Res. **5**(2), 023020 (2023).
[22]R. Cai, Y. Jin, Y. Li, J. Zhu, H. Zhu, T. Rabczuk, and X. Zhuang, J. Sound. Vibr. **555**, 117710 (2023).
[23]H. Haus and W. Huang, Proc. IEEE **79**(10), 1505–1518 (1991).
[24]E.-M. Graefe, A. A. Mailybaev, and N. Moiseyev, Phys. Rev. A **88**(3), 033842 (2013).